Classical and Quantum Dynamics – Project Report

Luboš Vrbka

J. Heyrovský Institute of Theoretical and Physical Chemistry
and
Faculty of Science, Department of Physical Chemistry
Charles University, Prague, Czech Republic

lubos.vrbka@jh-inst.cas.cz

Abstract

This report presents results of the calculations made as the final project for the course "Classical and Quantum Dynamics" held in the winter semester 2003 at the Faculty of Mathematics and Physics, Charles University, Prague. It covers both classical molecular dynamics and quantum dynamics results.

In the classical part, the binary mixture of Lennard–Jones particles (Argon and Krypton) is studied. The system is melted and evaporated and then let to freeze. The changes in the system are quantified using pair distribution functions and coordinate profiles for single particle. Surface properties of the particles are inspected using density profiles. Energy profiles are investigated, too.

Harmonic and Morse oscillator are studied using the quantum dynamics approach. Differences between real and imaginary time propagation are shown. Stationary states and energy spectra of these systems are calculated. Effect of the simulation conditions (initial wavefunction, length of the simulation, timestep) are studied and presented.

1 Classical Dynamics: Binary Mixture of Lennard–Jones Particles

1.1 Introduction

System of interest is the binary mixture of Lennard–Jones particles, i.e., particles interacting only via Lennard–Jones interactions. Potential for these interactions has the form

$$V_{ij} = 4\varepsilon_{ij}\left(\left(\frac{\sigma_{ij}}{r_{ij}}\right)^{12} - \left(\frac{\sigma_{ij}}{r_{ij}}\right)^{6}\right) \tag{1}$$

where r_{ij} is the separation between 2 interacting particles and σ_{ij} is the separation where the potential of such interacting particles is zero (not minimal!). The value of the potential ε_{ij} (potential minimum) corresponds to the separation of $\sqrt[6]{2}\sigma$. Argon (Ar) and Krypton (Kr), that can be treated as Lennard–Jones particles, were used in this study. Their parameters are given in the following table:

atom	Ar	Kr
mass [a.m.u.]	40	84
ε [kcal/mol]	1.0	1.4
σ [Å]	3.4	3.8

The values of ε and σ for non–homogenous pairs (i.e., for Argon – Krypton potential) are calculated as follows

$$\varepsilon_{ij} = \sqrt{\varepsilon_{ii}\varepsilon_{jj}} \tag{2}$$

$$\sigma_{ij} = \frac{\sigma_{ii} + \sigma_{jj}}{2} \tag{3}$$

1.2 "Experimental" Setup

Crystalline structure with dimensions $32.4 \times 32.4 \times 32.4$ Å^3 was created using program `makefcc`. Z–dimension of the simulation box was then changed to 97.2 Å. This operation formed the slab of particles surrounded by vacuum in the z–axis direction. The whole system was then equilibrated using molecular dynamics simulation program `cmdyn` in the NVT (canonical) ensemble with temperature held at $T = 75$ K (10 000 steps). The equilibrated sample was used as the initial structure for the 200 000 steps long production run. The same sample was also let to evaporate ($T = 200$ K) and the evaporated system was then cooled ($T = 10$ K) for the same number of steps to simulate a freezing process. All simulations used cutoff distance of size 14 Å and 0.005 ps timestep.

1.3 Results and Discussion

The resulting trajectories and other output files were processed using programs `a_gofr` (outputs pair distribution function for the system), `a_density` (provides density profiles along z–axis for both types of particles) and `a_singlecoor` (shows the evolution of the coordinates of a single particle in time).

The pair distribution function of the equilibrated sample (see Fig. 1) clearly indicates that the crystal structure melted. Shapes of the curves are characteristic for a Lennard–Jones liquid. The profile of the coordinates (see Fig. 2) of randomly chosen particle (number 600) also confirms the fact that the sample melted. Values are not correlated and change rapidly during the simulation. The vertical lines approximately in the middle of the simulation are

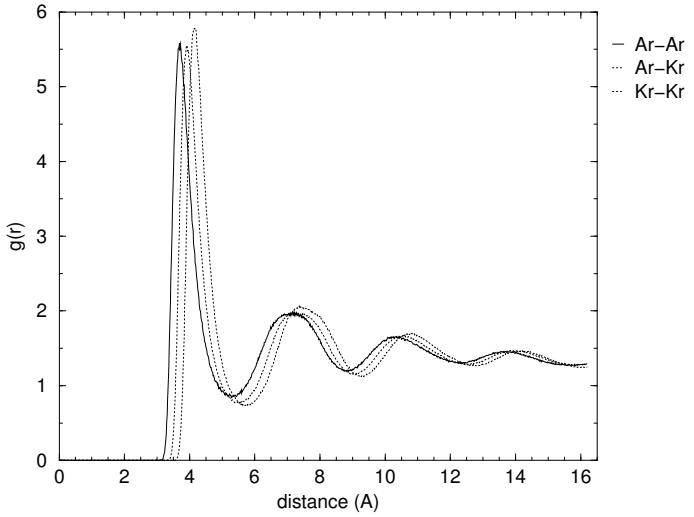

Figure 1: Pair distribution function for equilibrated sample

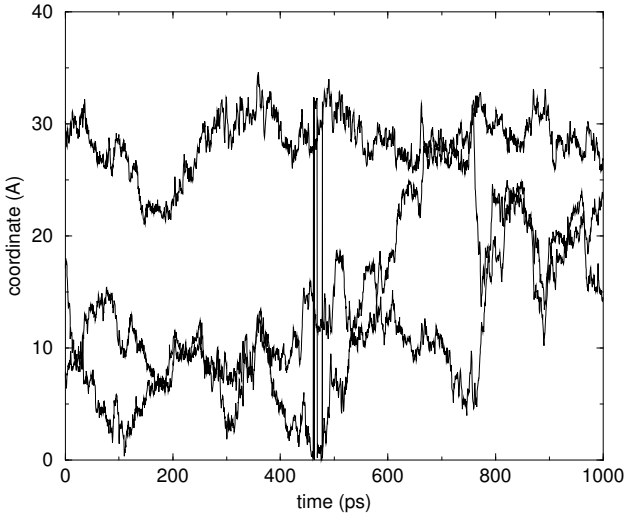

Figure 2: Single particle, coordinates evolution in time

the result of the "wrapping" of the atom (atom left the box and and entered it from the opposite side due to the periodic boundary conditions).

The density profile (see Fig. 3) shows that Ar exhibits surface excess in comparison with Kr. This result tells us that for the Ar–Kr binary mixture, Argon is a surfactant – species accumulating at the surface. This is probably direct consequence of the deeper minimum of the Lennard–Jones potential of the Krypton atoms. The whole system tends to possess the state with minimal energy, i.e., with each particle interacting with as many "neighbours" as possible. All particles therefore favor positions not exposed to the vacuum. Since potential of Argons is not so deep as the one of Kryptons, Argons are present at the surface with

higher probability – their presence at the surface brings smaller increase in the potential energy.

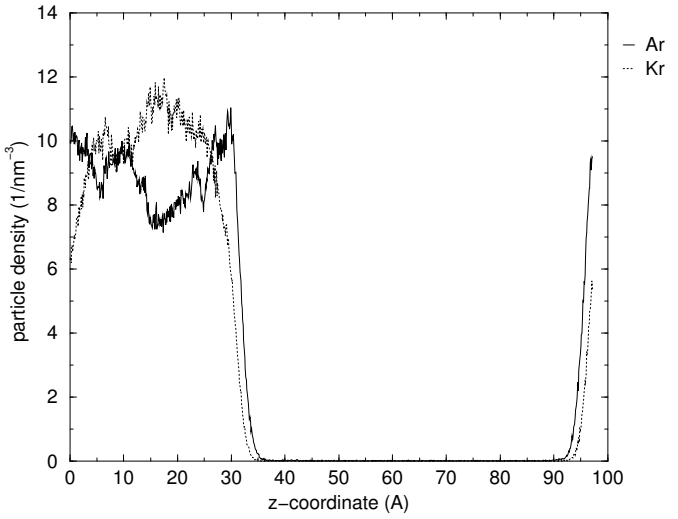

Figure 3: Density profile for production run

The pair distribution function and the coordinate profile for evaporated and frozen system are given in Figures 4, 5 and 6, 7, respectively.

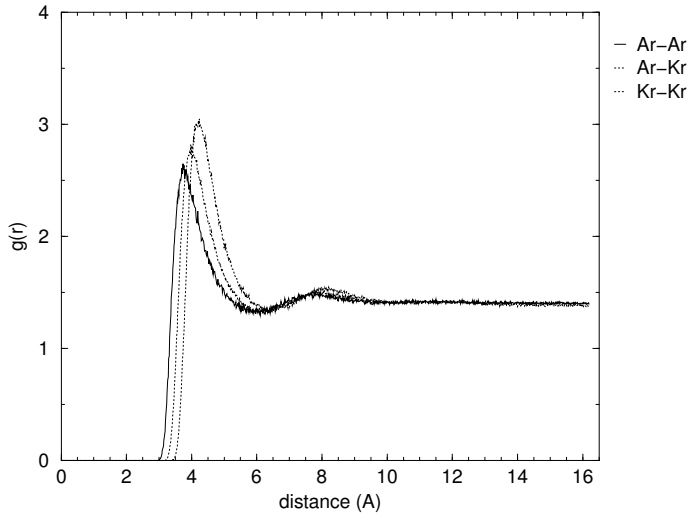

Figure 4: Pair distribution function for evaporated sample

The radical changes in the coordinate profiles for the evaporated sample clearly show that all particles are allowed to move freely, i.e., this system surely is in the gaseous state. The profiles for the system that was cooled down to low temperature exhibit changes only in the beginning of the cooling process. These changes can be assigned to reorganization of

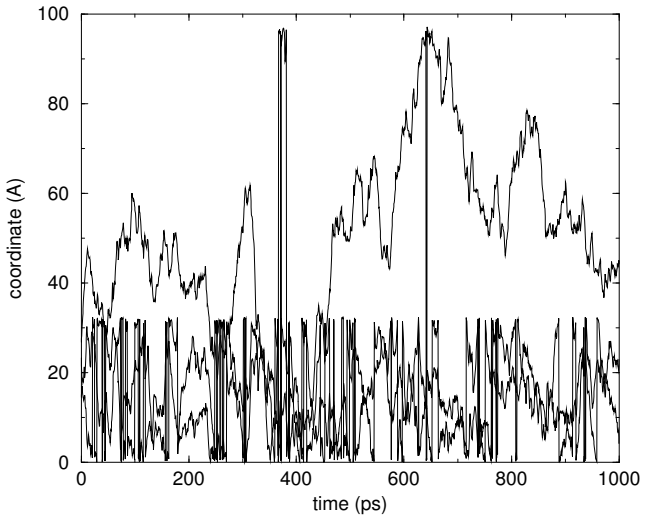

Figure 5: Single particle, coordinates evolution in time – vapour

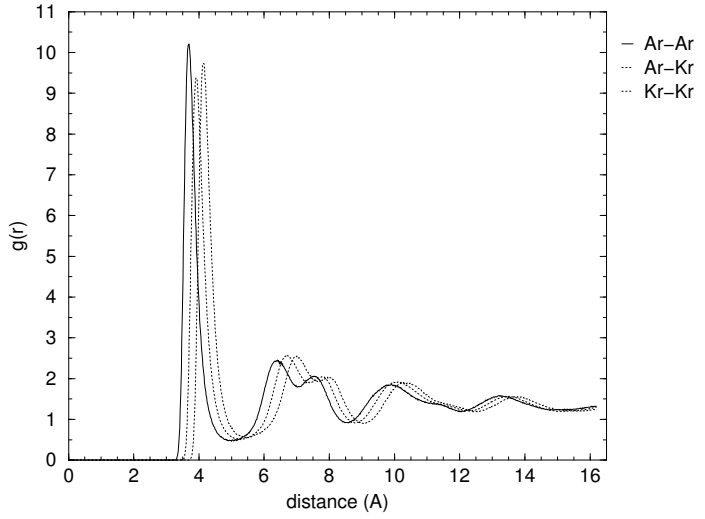

Figure 6: Pair distribution function for frozen sample

the particles during the transition from the gaseous to liquid and solid state (unlike in the gas phase, particles tend to stick together). After this initial period, the coordinate profiles for the frozen system remain constant with the small fluctuations only. These fluctuation arise from the vibrational motion of the particles in the solid (crystalline) structure.

The pair distribution functions for the evaporated and frozen system also confirm assumptions that were made in the previous paragraph. The largest peaks in the plots correspond to the minima of the Lennard–Jones interaction potentials. Almost constant function values for the evaporated sample confirm the uniform distribution of the particles in the simulation box, i.e., they prove that the system forms gaseous phase. The shapes of the

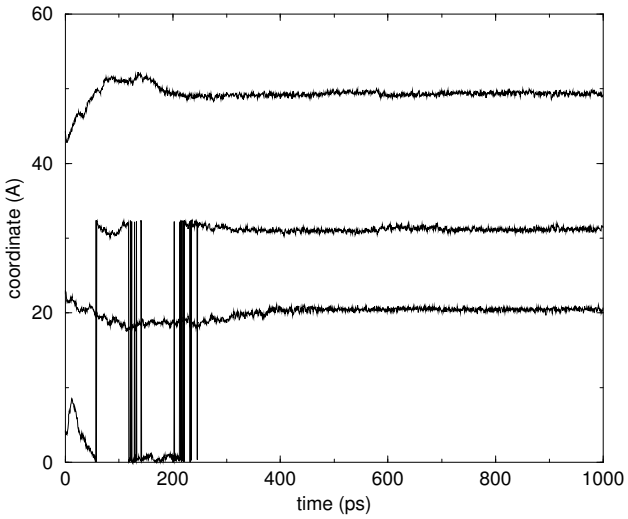

Figure 7: Single particle, coordinates evolution in time – solid

distribution functions for the frozen sample resemble the liquid sample results. The difference lies in the absolute value of the distribution functions. We can clearly see that values are higher than for the liquid system, i.e., that frozen system is more organized. The structure is not exactly crystalline, but longer simulation should lead to formation of (almost) perfect crystal.

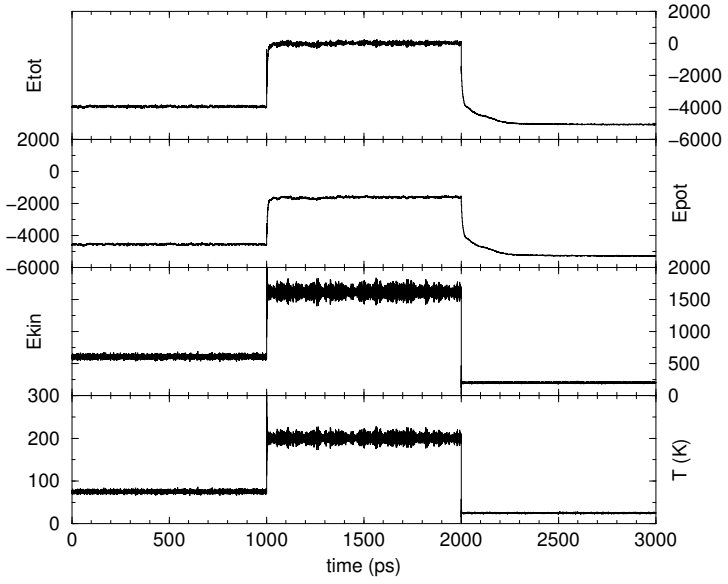

Figure 8: Energy and temperature profile

Changes in the energy and temperature during the simulations are depicted in Fig. 8. Graphs clearly show that the total energy of the system is given mainly by the potential

energy. Increasing the temperature in the evaporation simulation increases the kinetic energy that has the consequence in the increase of the potential energy due to higher frequency of particle collisions in the gaseous state. The temperature (and therefore also the kinetic energy) are held constant. As particles fill the whole box and the system equilibrates, the increase of the potential and total energy stops. This process is quite fast (takes few picoseconds). Similar behaviour can be observed for the freezing simulation. Decreasing the temperature decreases also the kinetic energy. The system is then finding the most favorable state for the specified temperature (the solid state). It can be observed on the potential and total energy profiles that this process is markedly slower (lasts approximately 300–400 ps) than the heating and evaporation. Particles are aggregating and finally form some kind of condensed phase that would turn to perfect crystal if very long simulation time would be used.

2 Quantum Dynamics : Morse Oscilator

2.1 Introduction

The **harmonic potential** (see Fig. 9) is given by

$$V(x) = \frac{1}{2}k(x - x_0)^2 \tag{4}$$

where k is the force constant (the second derivative of the potential V with respect to x) and x and x_0 are instantaneous and equilibrium displacements, respectively. The permitted energy levels are

$$E_n = \left(n + \frac{1}{2}\right)\hbar\omega \tag{5}$$

where

$$\omega = \sqrt{\frac{k}{m}} \tag{6}$$

is the **harmonic frequency** of the oscillator, m is the mass of the oscillator and n is the **vibrational quantum number**. The energy spectrum is an equally spaced ladder of the energy levels.

The **Morse potential** (see Fig. 9) that is defined by the Eq. (7) was introduced by Morse in 1929.[1] It is an empirical potential usually used for the description of chemical bond.

$$U(x) = D\left(1 - e^{-a(x-x_0)}\right)^2 \tag{7}$$

The labeling of the identical variables is the same as for the Harmonic potential. D is the depth of the potential minimum. The force constant for the Morse oscillator is

$$k \ = \frac{d^2U}{dx^2} = -2a^2D\left(e^{-a(x-x_0)} - 2e^{-2a(x-x_0)}\right) \tag{8}$$

[1] Morse P. M. *Phys.Rev.* **34** (1929) 57

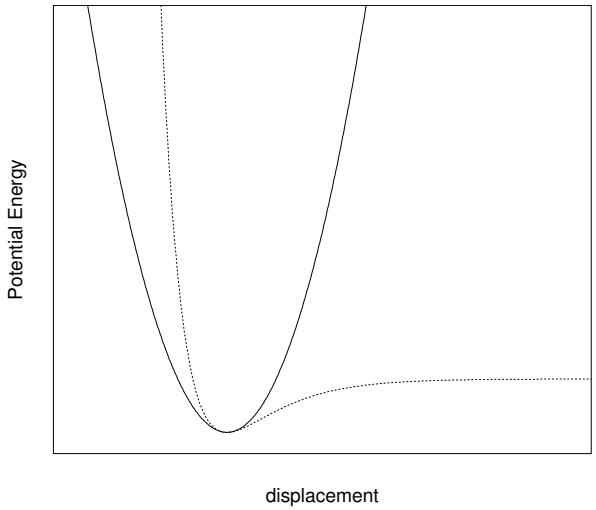

Figure 9: Shapes of the harmonic (solid line) and Morse (dotted line) potential

The Morse and harmonic potential fit to each other for small displacements from equilibrium where $(x - x_0)$ approaches zero. For such cases the term in the bracket is equal to -1 and the expression for the factor a is given by

$$a = \sqrt{\frac{k}{2D}} \tag{9}$$

The permitted energy levels for the Morse oscillator are usually calculated using perturbation theory correction to the harmonic oscillator energy and are given by

$$E_n = \left(n + \frac{1}{2}\right)\hbar\omega - \left(n + \frac{1}{2}\right)^2 \hbar\omega r \tag{10}$$

where r is the constant of anharmonicity that can be expressed as

$$r = \frac{a^2\hbar}{2m\omega} = \frac{\hbar\omega}{4D} \tag{11}$$

In case of Morse oscillator, spacing between energy levels is no more uniform. The gaps between levels gradually decrease with increasing n.

This study assumes that $m = 1$, $\hbar = 1$, $D = 2.5$ and $\omega = 1$. For given conditions, it is clear that the force constant value for the harmonic oscillator is

$$k \ = \omega^2 m = 1 \tag{12}$$

therefore a has to be

$$a = \sqrt{\frac{k}{2D}} = \sqrt{\frac{1}{2 \cdot 2.5}} = \frac{1}{\sqrt{5}} \tag{13}$$

for the results for both oscillators to be comparable.

2.2 Theoretical background

Quantum dynamics simulates behaviour of a particle(s) using the time–dependent Schrödinger equation

$$i\hbar\frac{\partial\Psi}{\partial t} = \mathcal{H}\Psi \tag{14}$$

where Ψ is wavefunction describing studied system and $\mathcal{H}$ is the Hamiltonian (operator of the total energy). The time evolution of the wavefunction Ψ, i.e. the solution of the Eq. (14) can be written as

$$\Psi(t) = \mathcal{U}\Psi(0) \tag{15}$$

where $\mathcal{U}$ is called **evolution operator**. For the **real time propagation** the evolution operator is

$$\mathcal{U} = e^{-\frac{i}{\hbar}\mathcal{H}t} \tag{16}$$

We can define the initial wavefunction $\Psi(0)$ as the linear combination of its eigenstates $|j\rangle$

$$\Psi = \sum_{j=0}^{\infty} c_j(0)\,|j\rangle \tag{17}$$

For the Hamiltonian in the exponent and its eigenfunction $|j\rangle$ we can write

$$f(\mathcal{H})\,|j\rangle = f(E_j)\,|j\rangle \tag{18}$$

We can prove equality (18) by writing operator $f(\mathcal{H})$ as expansion

$$f(\mathcal{H}) = \sum a_n\mathcal{H}^n \tag{19}$$

where a_n is some appropriate polynomial. Then, such operator acts on $|j\rangle$ as follows.

$$\sum a_n\mathcal{H}^n\,|j\rangle = \cdots + a_nE_j\underbrace{\mathcal{H}\cdots\mathcal{H}}_{n-1}|j\rangle + \cdots = \sum a_nE_j^n\,|j\rangle = f(E_j)\,|j\rangle \tag{20}$$

The result is exactly the same as in the Eq. (18).

Now, from Eqns. (15) and (16) we can write

$$\sum_{j=0}^{\infty} c_j(t)\,|j\rangle = \sum_{j=0}^{\infty} c_j(0)e^{-\frac{i}{\hbar}E_jt}\,|j\rangle \tag{21}$$

The evolution of the expansion coefficients c_j (complex numbers) in the real time propagation therefore can be written as

$$c_j(t) = c_j(0)e^{-\frac{i}{\hbar}E_jt} \tag{22}$$

The evolution operator for the **imaginary time propagation** has got slightly different form

$$\mathcal{U} = e^{-\frac{1}{\hbar}\mathcal{H}t} \tag{23}$$

i.e., the exponent in the real time propagator is multiplied by $-i$ to yield imaginary time propagator. For this type of propagation, the formula for the evolution of the expansion coefficients c_j is

$$c_j(t) = c_j(0)e^{-\frac{1}{\hbar}E_j t} \tag{24}$$

We can now use following substitution to simplify the exponents the Equations (22) and (24)

$$x = \frac{1}{\hbar}E_j t \tag{25}$$

The exponential term in the real time propagation can then be written as

$$e^{-ix} = \cos x - i \sin x \tag{26}$$

that is constant, non–decaying function, i.e., the modulus (absolute value) of the expansion coefficient remains constant. Real and imaginary part of the expansion coefficient evolve with `sinus` and `cosinus` functions, respectively. Since e^{-x} is decaying function, it is clear that in the imaginary time propagation the expansion coefficients decay. The rate of this decay depends on the energy of the eigenstate the coefficient belongs to, i.e., for higher states the decay is faster. After sufficiently long time, coefficients of all states but one ($|0\rangle$) are zero. This means that imaginary time propagation provides us with the lowest stationary state (ground state) $|0\rangle$. When we have this state, we can project it out from the wavefunction (project the wavefunction of the dimensionality n to the perpendicular (orthogonal) subspace with dimensionality $n-1$) and by repeating of the same routine, we get the next stationary state $|1\rangle$.

To prove the correctness of the previous statement about subtracting the lowest state from the wavefuction, let us assume vector $\vec{v}$ that can be written as a sum of two other, mutually perpendicular vectors $\alpha\vec{u}$ and $\beta\vec{u}^{\perp}$ so that

$$\vec{v} = \alpha\vec{u} + \beta\vec{u}^{\perp} \tag{27}$$

The projection of the vector $\vec{v}$ into the direction of the vector $\vec{u}$ can be expressed as

$$\alpha\vec{u} = |\vec{v}| \cos\varphi \frac{\vec{u}}{|\vec{u}|} = |\vec{v}| \frac{\vec{u}\cdot\vec{v}}{|\vec{u}|\,|\vec{v}|}\frac{\vec{u}}{|\vec{u}|} = \frac{(\vec{u}\cdot\vec{v})\,\vec{u}}{|\vec{u}|^2} \tag{28}$$

where φ is the angle between $\vec{v}$ and $\vec{u}$. We can therefore write

$$\beta\vec{u}^{\perp} = \vec{v} - \alpha\vec{u} = \vec{v} - \frac{(\vec{u}\cdot\vec{v})\,\vec{u}}{|\vec{u}|^2} \tag{29}$$

When we apply the same approach in the quantum formalism, we get

$$\Phi = \Psi - \frac{\langle\Psi|0\rangle\,|0\rangle}{|0\rangle^2} = \Psi - \frac{c_0|0\rangle}{|0\rangle^2} = \sum_{j=0}^{\infty} c_j\,|j\rangle - c_0\,|0\rangle = \sum_{j=1}^{\infty} c_j\,|j\rangle \tag{30}$$

i.e., Φ is a new wavefunction that does not contain the ground state of the wavefunction Ψ. Functions Ψ and Φ are orthogonal and the dimensionality of the Φ is the dimensionality of the function Ψ decreased by 1, i.e. we projected the ground state of the Ψ out of Φ. The lowest stationary state of the Φ wavefuction corresponds to the first excited state of the wavefunction Ψ.

When using real time propagation, it is convenient to calculate so called **autocorrelation function** defined as

$$C(t) = \langle \Psi(0) | \Psi(t) \rangle \tag{31}$$

It provides information about the change in the spatial and phase relationships in the wavefunction and via the **Fourier Transform** is connected with measurable and observable spectra. We can write

$$C(t) = \sum_l \sum_j c_l^*(0) \langle l | \cdot c_j(0) | j \rangle e^{-\frac{i}{\hbar} E_j t} \tag{32}$$

Because eigenfunctions $\langle j|$ and $|l\rangle$ are othonormal, we can introduce the **Kronecker delta function** $\delta_{\mathbf{ij}}$ and then further simplify the expression

$$C(t) = \sum_l \sum_j c_l^*(0) c_j(0) \delta_{lj} e^{-\frac{i}{\hbar} E_j t} = \sum_j |c_j|^2 e^{-\frac{i}{\hbar} E_j t} \tag{33}$$

We can now proceed with the inverse Fourier transform (from time to frequency domain)

$$g(\omega) = N \int_{-\infty}^{\infty} C(t) e^{i\omega t} dt = N \sum_j |c_j|^2 \int_{-\infty}^{\infty} e^{it\left(-\frac{E_j}{\hbar} + \omega\right)} dt = N \sum_j |c_j|^2 \int_{-\infty}^{\infty} e^{it(\omega - \omega_j)} dt \tag{34}$$

where N contains some constants. It is possible to show that the solution of the integral in the Eq. (34) is so called **Dirac delta function** δ, an infinitely narrow peak at the frequency value ω_j. The result of the inverse Fourier transform of the autocorrelation function is therefore a spectrum (set of peaks) corresponding to the eigenstates of the wavefunction

$$g(\omega) = N \sum_j |c_j|^2 \delta(\omega - \omega_j) \tag{35}$$

2.3 "Experimental" Setup

All the input files were prepared using the Perl script `makepsi`. The quantum dynamics simulations themselves were performed with program `qrun`. `waveplot` program was used for the visualization of results.

Firstly, imaginary time propagation was set (keyword propa imag) and 10 low–lying stationary vibrational states of the harmonic and Morse oscillator were calculated. The time propagation type was then set to real (keyword propa real). The resulting autocorrelation functions were then transformed to spectral information using utility `acf2spec`. To see the effect of the timestep size and length of the simulation on the resulting spectrum, following combinations of parameters were used:

- 1 000 steps; timestep 0.01
- 5 000 steps; timestep 0.01
- 10 000 steps; timestep 0.01
- 20 000 steps; timestep 0.01
- 100 000 steps; timestep 0.001
- 10 000 steps; timestep 0.01
- 2 000 steps; timestep 0.05
- 1 000 steps; timestep 0.1

To see the effect of the initial conditions on the resulting spectra, several calculations were also started from the stationary states, i.e., wavefunctions corresponding to the stationary states were used as the initial conditions for the quantum dynamics program.

2.4 Results and Discussion

Following table summarizes results for the energies of the low–lying vibration modes for harmonic and Morse oscillator.

	total energy			
mode	harmonic	analytical	Morse	analytical
0	0.50000	0.50000	0.47500	0.47500
1	1.50000	1.50000	1.27506	1.27500
2	2.50000	2.50000	1.87562	1.87500
3	3.50000	3.50000	2.28007	2.27500
4	4.50000	4.50000	2.50484	2.47500
5	5.50000	5.50000	2.59690	2.47500
6	6.50000	6.50000	2.62486	2.27500
7	7.50000	7.50000	2.63824	1.87500
8	8.50000	8.50000	2.69536	1.27500
9	9.50000	9.50000	2.82101	0.47500

It is clear from the results that both oscillators are comparable only for the lowest states, that is consistent with assumptions made in the Introduction. Analytical energies compare well with the results for the harmonic oscillator. Energy values for the Morse oscillator are well comparable to the analytical solutions up to the vibration level corresponding to the vibrational quantum number $n = 4$. Following states belong to continuum of energies, i.e.,

their energy is larger than the potential depth D. Discretization of the wavefunction brings an artefact here, because states belonging to continuum are being reported as vibrational states with higher n.

Wavefunctions corresponging to the 10 lowest vibrational states of the harmonic and Morse oscillator are plotted in Fig. 10. It can be clearly seen that with increasing n the differences

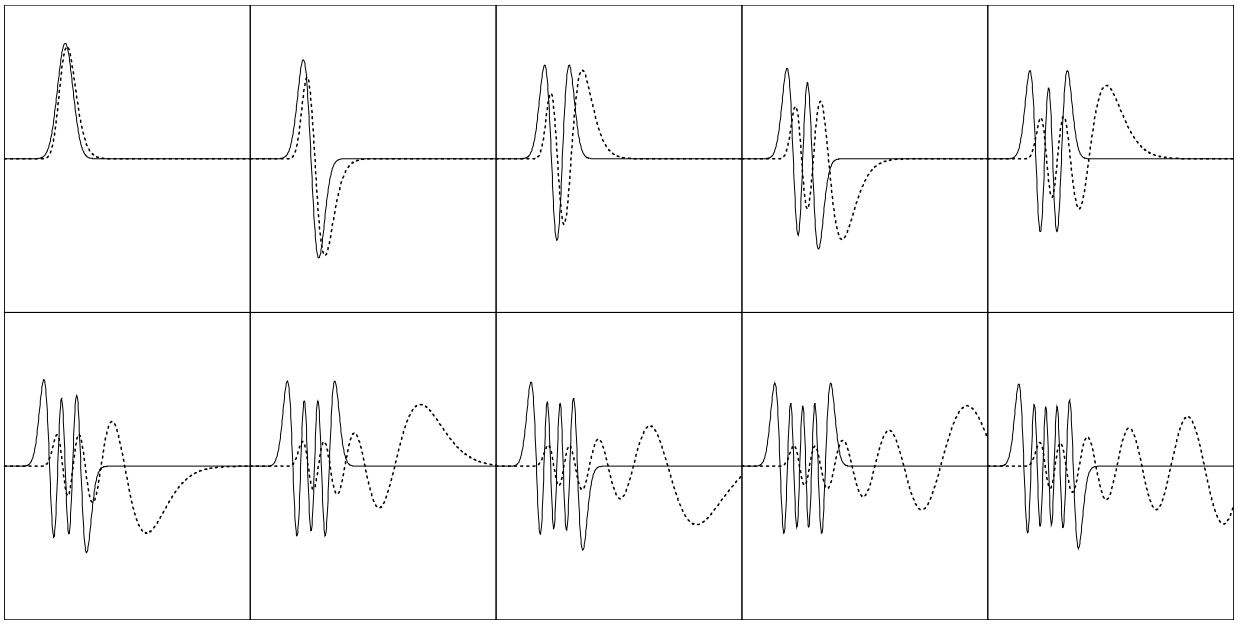

Figure 10: Wafefunctions of 10 lowest energy states of the harmonic (solid line) and Morse (dotted line) oscillator

between these two oscillators increase. The asymmetry in the Morse oscillator wavefunctions is the direct consequence of the asymmetry of the potential. The probability density decreases with increasing potential, i.e., the steeper (harder) potential that the wavefunction experiences for small displacements causes the probability density to decrease in comparison with the large displacements where the potential is much softer. Note that states with $n > 4$ for this case of Morse oscillator in fact do not exist. The reason was discussed in the previous paragraph.

Figures 11 and 12 illustrate the effect of the length of the simulation and the timestep size, respectively, on the spectra calculated from autocorrelation functions. The resolution of the peaks increases with longer simulations. Better resolution can be also achieved by using small timestep, but adequately larger number of timesteps has to be used, i.e., the product nsteps $\times$ timestep is constant.

Use of the shorter timestep also extends the spectrum in the energy (frequency) domain. This phenomenon is connected to the so called **Nyquist theorem**. This theorem states that when a wavefunction is discretized (wavefunction evolves in discrete time intervals given by the timestep τ), only the vibrational modes in the wavefunction that have frequency below half of the **sampling frequency** $(1/\tau)$ will be recorded, because in order to

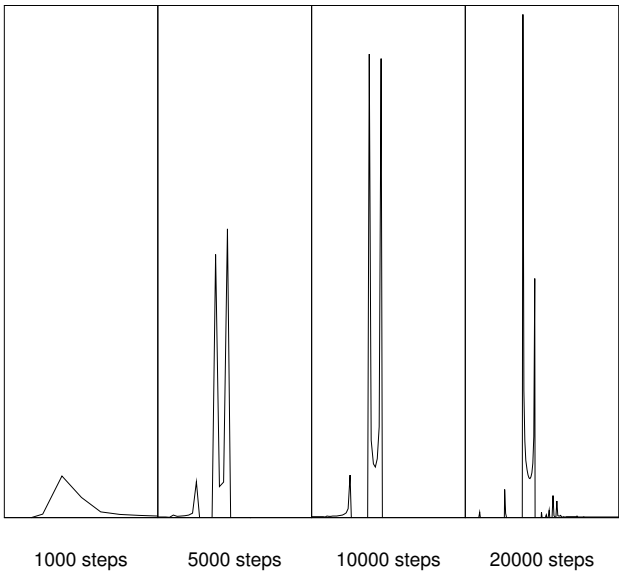

Figure 11: Calculated spectra – constant timestep (0.01), variable length of the simulation

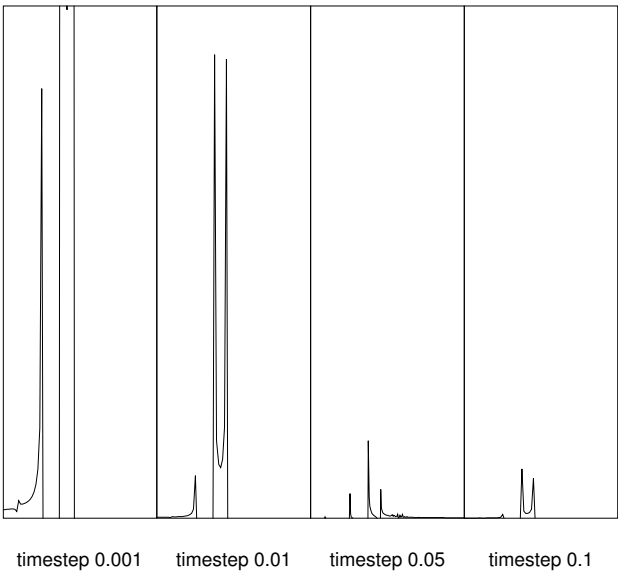

Figure 12: Calculated spectra – constant simulation time, variable timestep

properly describe a vibrational mode, sufficient samples (at least two) have to be recorded to capture its peaks and throughs. As higher vibrational states correspond to higher energy, their waveforms oscillate faster, therefore we can properly describe them only by sampling the value of the wavefunction in shorter time intervals τ.

Wavefunction corresponding to some stationary state (defined by the vibrational quantum number n) has the moduli (absolute values) of all expansion coefficients c_j but one equal

to zero (see Eq. 17). Only the modulus of the coefficient c_n corresponding to eigenstate $|n\rangle$ equals to 1. Equations 22 and 26 then imply, that only the real and imaginary part of the coefficient c_n evolve, values for all other coefficients remain zero. Spectra obtained for such simulations therefore contain always only single peak corresponding to the energy of the initial eigenstate $|n\rangle$.

Acknowledgement

Author would like to Mgr. Martin Mucha for his time that he spent with me during consultations and for providing me with priceless information.